Optimizing autologous bone contribution to implant osseointegration

Benjamin R. Coyac, DDS, PhD[*], **Qiang Sun, MD, PhD**[*,†], **Brian Leahy, BSc**[*], **Giuseppe Salvi, BSc**[*], **Xue Yuan, PhD**[*], **John B. Brunski, PhD**[*], **Jill A. Helms, DDS, PhD**[*]

[*]Department of Plastic and Reconstructive Surgery, School of Medicine, Stanford University, Palo Alto, California 94304, United States of America

[†]Department of Plastic Surgery, China Medical University Hospital, Shenyang, 110001, China

Abstract

Background—Autologous bone can be harvested from the flutes of a conventional drill or from a bone scraper; here we compared whether autologous bone chips generated by a new slow-speed instrument were more osteogenic than the bone chips generated by conventional drills or bone scrapers. Additionally, we tested whether the osteogenic potential of bone chips could be further improved by exposure to a WNT therapeutic.

Methods—Osteotomies were prepared in fresh rat maxillary first molar extraction sockets using a conventional drill or a new osseo-shaping instrument; titanium alloy implants were placed immediately thereafter. Using molecular/cellular and histologic analyses, the fates of the resulting bone chips were analyzed. To test whether increasing WNT signaling improved osteogenesis in an immediate post-extraction implant environment, a WNT therapeutic was introduced at the time of implant placement.

Results—Bone collected from a conventional drill exhibited extensive apoptosis; in contrast, bone generated by the new instrument remained *in situ*, which preserved their viability. Also preserved was the viability of the osteoprogenitor cells attached to the bone chips. Exogenous treatment with a WNT therapeutic increased the rate of osteogenesis around immediate post-extraction implants.

Conclusions—Compared with conventional drills or bone scrapers, a new cutting instrument enabled concomitant site preparation with autologous bone chip collection. Histology/histomorphometric analyses revealed that the bone chips generated by this new tool were more osteogenic and could be further enhanced by exposure to a WNT therapeutic. Even though gaps still existed in L-PBS and L-WNT3A cases, the area of peri-implant bone was significantly greater in L-WNT3A treated sites.

One-sentence summary describing the key findings from the study

Corresponding author: J.A. Helms, Stanford University, 1651 Page Mill Road, Palo Alto, California 94304, United States of America. Phone number: +1 650 736 0919. Fax number: +1 650 736 4374. jhelms@stanford.edu.
Authors' roles
Study design: BRC and JAH. Study conduct: BRC. Data collection: BRC, QS, BL, GS, XY, JBB. Data analysis: BRC, JBB and JAH. Data interpretation: BRC, JBB and JAH. Drafting manuscript: BRC and JAH. Revising manuscript content: all authors. Approving final version of manuscript: all authors. All authors take responsibility for the integrity of the data analysis.

We present clinically relevant methods for preserving the viability of autologous bone chips and enhancing their direct contribution to immediate post-extraction implant osseointegration via Wnt pathway activation.

Keywords

Autograft; Grafting, Bone; Regeneration; Osteogenesis; Wnt proteins; Osteotomy

Introduction

Local bone graft can be obtained during routine surgical procedures and used to repair osseous defects if handled properly[1, 2]. Compared to cortical bone, cancellous bone is preferable as graft material[3, 4] because of its cellularity[5]. The mineralized matrix of the graft also acts as a nidus for osteoclast attachment; these osteoclasts resorb the matrix and create new attachment sites for osteoblasts (reviewed in Baron et al.[6]). Whether the mineralized matrix must be fully resorbed prior to the onset of new bone is not entirely clear; theoretically, the smaller the particle size of the mineralized matrix, the more rapid would be the resorption process, and the subsequent onset of new bone formation[7]. This theory has been validated *in vitro*[8] and *ex vivo*[9], but has not been fully tested *in vivo*[10].

Bone grafts are often used in immediate post-extraction implant situations, where the gap around the implant is larger than the volume of the implant itself; in such cases, bone remodeling is extensive, and the final crestal bone level can be unpredictable[11–13]. To increase predictability, the gap is typically filled with bone debris[14–16] and the faster new bone forms in the gaps, the less chance there is for crestal resorption[17]. The volume of bone debris generated during osteotomy site preparation may be insufficient to fill a defect and, in these cases, surgeons often turn to the use of bone graft substitutes and extenders[18]. These fillers include decellularized and in some cases, demineralized and/or deproteinized cadaveric or xenogeneic bone[19], which when mixed with autologous material, create a larger volume of mineralized matrix to place around implants. These substitute materials, however, do not contain cells nor do they contain measurable amounts of active growth factors, despite claims to the contrary[20].

If methods could be developed that optimized the amount, viability, and osteogenic potential of autologous bone chips, then the use of synthetic materials and other void fillers could be eliminated, or at least reduced. In a previous work, we explored the use of an ultra-low-speed, irrigation-free instrument, the OsseoShaper (Nobel Biocare, Switzerland), for osteotomy site preparation. When compared to osteotomies generated with conventional drills, osteotomies produced with a miniaturized version of this osseo-shaping instrument exhibited significantly better bone viability[21], which was attributable to the minimal heat generated during bone cutting[21].

Whether the viability of the osteotomy site directly translated into faster peri-implant bone formation, however, has not been demonstrated. Here, we focused on the short-, intermediate- and long-term fate(s) of the bone chips generated by a miniaturized osseo-shaping instrument, specifically in the environment of an immediate post-extraction implant.

We directly compared the viability of bone chips generated by the osseo-shaping instrument to bone chips generated by conventional drills, and by manual bone scrapers. Based on findings from these studies, we then tested liposomal WNT3A (L-WNT3A) as a potential therapeutic for enhancing the bone-forming capacity of viable bone chips generated during osteotomy site preparation.

Materials and methods

Animals

Stanford Committee on Animal Research approved the protocol used here (APLAC #13146), which conforms to ARRIVE guidelines[22]. In total, 30 five-week-old female Sprague-Dawley rats (Charles River Laboratories, Wilmington, MA) and 6 $Axin2^{CreERT2/+};R26R^{mTmG/+}$ mice (Nos. 018867 and 007576, respectively, Jackson Laboratories, Bar Harbor, ME) were used in this study. The $Axin2^{CreERT2/+};R26R^{mTmG/+}$ strain was used to identify the distribution of WNT-responsive stem cells [23] and their contribution to bone healing and implant osseointegration. To induce Cre expression in $Axin2^{CreERT2/+};R26R^{mTmG/+}$ reporter mice, tamoxifen (4 mg/25 g body weight) was delivered via intraperitoneal (IP) injection. Mice were sacrificed at timepoints indicated, and GFP immunostaining was used to identify Wnt-responsive stem cells and their progeny.

In vitro cell-based apoptosis assays

Caspase3 is activated in apoptotic cells[24] and its role in the apoptotic pathway has been well characterized (reviewed in[25]). To validate Caspase3 activity as a proxy for measuring apoptosis in bone grafts, freshly isolated bone marrow stromal cells (BMSCs) were harvested from donor mice [26, 27] and exposed to the cytotoxic agent Camptothesin[28] to induce apoptosis in a dose-dependent manner.

Caspase activity was then measured in the BMSCs following Camptothesin treatment, using spectrophotometric detection of the cleavage products of chromophore p-nitroanilide (pNA) from Ac-DEVD-pNA, in accordance with the manufacturer's instructions (Caspase 3 assay kit, Abcam, CA, USA). Cleavage products were detected at 405nm wavelength using a microplate reader (PerkinElmer, USA) (see Supplementary Figure 1 in online Journal of Periodontology). The same method of measuring Caspase 3 activity was then used to quantify apoptosis in a bone graft as a function of time.

Surgeries

For rats undergoing surgeries, anesthesia was administered via IP injection of Ketamine (68 mg/kg) and Xylazine (6.8 mg/kg); analgesia was provided via subcutaneous injection of Buprenorphine-SR (0.5 mg/kg). For mice undergoing surgeries, anesthesia was provided by a Ketamine (80 mg/kg)/Xylazine (8 mg/kg) cocktail administrated via IP injection; analgesia was ensured via subcutaneous injection of Buprenorphine-SR (0.1 mg/kg). During recovery, rodents recovered on heated pads; after full recovery, rodents were housed in a temperature-controlled environment with 12-h light/dark cycles and were fed an ad libitum diet. Weight changes were <5%. No adverse events (e.g., uncontrolled pain, infection, prolonged inflammation) were encountered.

Ovariectomy

To perform ovariectomy (OVX), 6-week-old rodents were acclimated for one week then anesthetized as described above. A dorsal midline incision was made between the mid-back and tail base. The peritoneal cavity was accessed through bilateral muscle layer incisions, the ovary was identified, the connection between the fallopian tube and the uterine horn was suture-ligated. After removal of both ovaries, wounds were closed layer by layer[29].

Tooth extraction, osteotomy site preparation, implant characteristics, and implant placement

Eight weeks after OVX, rodents underwent bilateral maxillary first molars (mxM1) extraction using curved forceps, followed by osteotomy site preparation and immediate post-extraction implant placement. Using a dental handpiece (KaVo Dental, UK) with saline irrigation, a pilot hole was produced in the furcation area of the fresh extraction socket. Osteotomies in rats were then enlarged with a miniaturized version of the osseo-shaping instrument, following which miniaturized tri-oval implants were placed (Table 1). All implants were positioned below the level of the occlusal plane. Osteotomies in mice were produced following an identical protocol, using smaller implants (0.62 mm external diameter, titanium-6 Aluminium-4 Vanadium alloy "Retopins"; NTI Kahla GmbH, Germany). After implant placement, a periosteal flap was repositioned to achieve closure.

Sub-renal capsule transplantation

In rodents, autografting is unnecessarily stressful; consequently, a syngeneic transplantation strategy was employed[30], in which the donor and host have identical genetic backgrounds; consequently, tissues are immunologically compatible and transplantation does not elicit an immune response[31]. For example, some bone grafts were transplanted to the sub-renal capsule (SRC[32]). The SRC allows for a detailed examination of organogenesis and tissue development[33], including bone growth[34] as the environment is highly vascular yet does not make a direct cellular contribution to the bone formation process[33]. Details about sub-renal capsule transplantation can be found in Supplementary Materials and Methods in online Journal of Periodontology.

L-WNT3A and L-PBS preparation and delivery

Liposomes reconstituted with WNT3A (L-WNT3A) were prepared as previously described[36]. In brief, purified human recombinant WNT3A (Ankasa Regenerative Therapeutics, Inc., South San Francisco, CA) was solubilized in 1% CHAPS at a final concentration of 40 ng/μL. The WNT3A solution was then combined with preformed liposomes made with DMPC/cholesterol (90:10) (Avanti polar lipids, Alabaster, AL) by extrusion. In those cases where implants were treated with L-WNT3A or an identical liposomal formulation containing phosphate buffered saline (L-PBS), a split-mouth design was employed. In all cases, a ~15 μL volume of the relevant solution was deposited into the osteotomy/fresh extraction socket. Details about L-WNT3A and L-PBS preparation and delivery can be found in Supplementary Materials and Methods in online Journal of Periodontology.

Imaging

A μCT tomography data-acquisition system (VivaCT 40, Scanco, Brüttisellen, Switzerland) at 10.5μm voxel size (70kV, 115μA, 300ms integration time) was used for scanning and reconstruction. Bone morphometry was performed using acquisition system's analysis software (Scanco Medical AG, Bassersdorf, Switzerland). Multiplanar reconstruction and volume rendering were carried out using Avizo (FEI, Hillsboro, OR) and ImageJ (NIH, Bethesda, MD) software. Images were organized using Adobe Illustrator (Adobe, San Jose, CA).

Finite Element Methods

COMSOL Multiphysics 5.4 was used to calculate the total volume of the gap between the implant and socket walls. A CAD file of the implant was imported into Comsol, then virtually installed into a 3D model of an osteotomy prepared using the osseo-shaping instrument. The osteotomy was located in the inter-radicular bone of mxM1, which was represented in Comsol based on μCT data acquisition. Details about Finite Element Methods can be found in Supplementary Materials and Methods in online Journal of Periodontology.

Tissue processing

After harvest, samples were fixed in 4% paraformaldehyde (PFA), decalcified in 10% EDTA solution at 25°C for a minimum of two weeks under constant microwave irradiation. The samples were then dehydrated using an ascending graded ethanol series and embedded into paraffin blocks for sectioning. Sections were generated at an 8-μm thickness by a Leica microtome (Leica Instruments GmbH, Hubloch, Germany).

Before histological staining, paraffin sections were de-paraffinized in Citrisolv (Decon Labs Inc. PA), and hydrated via a descending graded ethanol series. After staining, sections were dehydrated in a graded series of ethanol and Citrisolv, and subsequently cover-slipped with Permount (Fisher Scientific) mounting media.

For Aniline blue staining, slides were treated with a saturated solution of picric acid, followed by a 5% Phosphotungstic acid solution and 1% Aniline blue staining.

Enzymatic assays

To detect alkaline phosphatase (ALP) activity, tissue sections were treated with ALP-detection solution containing BCIP (5-bromo-4-chloro-3-indolyl phosphate; Roche, #11383221001) and NBT (nitro blue tetrazolium chloride; Roche, #11383213001) at 37°C for 30 mins according to the manufacturer's instructions. TRAP activity was observed using a leukocyte acid phosphatase staining kit (#386A-1KT, Sigma-Aldrich, St. Louis, MO). Tissue sections were processed according to the manufacturer's instructions.

Immunostaining

Tissue sections were permeabilized with 0.5% Tween20. After antigen retrieval, slides were blocked with 5% goat serum (Vector S-1000) for 1h at room temperature and incubated with primary antibodies overnight at 4°C. After washing with PBS, slides were incubated with Cyanine5 conjugated goat anti-rabbit secondary antibody (Invitrogen, A10523) for 30

minutes, then mounted with DAPI mounting medium (Vector Laboratories). Primary antibodies included antibodies against the osteoprogenitor cell markers Runx2 (ab192256, Abcam, used at a dilution of 1:1000) and Osterix (ab22552, Abcam; used at a dilution of 1:100;), antibodies against the cell proliferation markers PCNA (ab18197, Abcam; used at a dilution of 1:2000) and Ki67 (ab15580, Abcam; 1:100), an antibody to recognize the osteoblast marker collagen type I (ab34710, Abcam; used at a dilution of 1:500), anti-GFP (Cell Signaling Technology, 2956T; used at a dilution of 1:500).

TUNEL staining

For programmed cell death analysis, the slides were labeled using TUNEL kit (Roche, Indianapolis, IN) according to manufacturer's instructions.

Histomorphometric analysis

Histomorphometric measurements were performed using ImageJ software (NIH, Bethesda, MD). A minimum of 3 implant sites was analyzed at each time point (Table 2). For each implant site, a minimum of three aniline blue-stained histologic sections in the transverse plane, that spanned the distance from the crestal to the apical aspects of the alveolar plates, were used to quantify the proportion of bone in the peri-implant region. The peri-implant region was defined as the area extending from the implant outer surface and encompassing the extraction socket gaps. Each section was photographed using a Leica digital image system at 20x magnification.

Statistical analysis

Mann-Whitney U test was used for group comparisons with the R 3.3.2 software. Differences between groups were considered significant when $p < 0.05$. Details about the Statistical Analysis can be found in Supplementary Materials and Methods in online Journal of Periodontology.

Results

Conventional handling methods do not prioritize the viability of autologous bone chips

Autologous bone chips have inherent osteogenic potential, prompting clinicians to collect this osseous coagulum for reconstructive purposes. Clinicians attempt to collect from osteotomy drills, but the particles tend to be small and therefore are minimally retained (Fig. 1A). Another confounding variable is that this material is collected, then held outside the body i.e., *ex vivo*, where it immediately begins to undergo programmed cell death, as shown by TUNEL staining (Fig. 1B). A quantitative method to measure programmed cell death [24] was employed: in bone chips that were held outside the body, Caspase 3 enzymatic activity significantly increased as a function of time (Fig. 1C). In addition to apoptosis, cells attached to the bone chips ceased proliferation (compare left panel, PCNA expression at time of harvest with right panel versus 1h after harvest, Fig. 1D).

In contrast to conventional drills, the osseo-shaping instrument has a cutting flute running its length; upon advancement bone chips are collected in the clockwise-rotating flutes (Fig. 1E). When the instrument is withdrawn, the rotation is reversed and bone chips are deposited

back in the osteotomy site; these *in vivo* bone chips showed minimal evidence of programmed cell death (Fig. 1F). The osseo-shaping instrument also cuts at very low (50rpm) speeds; consequently, osteocytes in the resulting bone chips remained viable (Fig. 1G) and continued to express the osteoprogenitor cell marker, Osterix (Fig. 1H).

Compared to chips produced by bone scrapers, chips produced by an osseo-shaping instrument are more osteogenic

bone chips are generated by scraping cortical bone surfaces e.g., the ramus or the menton [37]. Bone scraper-generated bone chips are comprised of dense lamellar cortical bone (Fig. 2A). In comparison, bone chips generated by the osseo-shaping instrument are largely cancellous (Fig. 2B). We compared the osteogenic potential of bone chips produced by scrapers with those generated by the osseo-shaping instrument by transplanting the materials to the sub-renal capsule (SRC). In this *ex vivo* environment, the behavior of the transplanted material could be assessed without contribution from cells other than those in the graft itself. After 7 days, bone scraper material appeared unchanged from the time of transplantation (Fig. 2C). In contrast, material generated by the osseo-shaping instrument was embedded and surrounded by new bone (asterisks, Fig. 2D). While osteocytes in the scraped bone material were non-viable, as shown by the absence of DAPI^{+ve} staining in the osteocyte lacunae (Fig. 2E), osteocytes in the material generated by the osseo-shaping instrument were, in many cases, still viable (Fig. 2F). Another difference between the material generated by scraping versus the osseo-shaping instrument was the absence of cells attached to the scraped material and the presence of viable cells attached to the material generated by the osseo-shaping instrument.

The material produced by an osseo-shaping instrument gives rise to new peri-implant bone

In the next experiments, we focused on the *in vivo* fate of the material generated by the osseo-shaping instrument. Because bone chips generated by conventional drills are washed away with the copious irrigation used, an *in vivo*, side-by-side analysis was not possible.

One measure of cell viability is mitotic activity[26]; cells attached to the material generated by the osseo-shaping instrument showed widespread Ki67 expression on post-implant day 3 (Fig. 1G). Co-expression of the osteogenic transcription factors Runx2 (Fig. 2H) and Osterix (Fig. 2I) confirmed the onset of new bone formation around bone chips generated by the osseo-shaping instrument. Analyses on post-implant day 7 showed widespread expression of the osteogenic protein Collagen type I (Fig. 2J) along with extensive ALP activity (Fig. 2K). ALP activity was coupled with TRAP activity (Fig. 2L), indicating that the mineralized matrix of the bone chips was undergoing remodeling.

To demonstrate the origin of the new bone matrix, a SRC transplantation assay was employed. At the time of initial transplantation, bone chips, identified by aniline blue staining, were surrounded by undifferentiated cells (Fig. 2L); after 7 days, the bone chips were surrounded by new bone matrix (asterisks, Fig. 2M).

To definitively demonstrate that new arose from the cells attached to bone chips, the material were harvested from a Wnt reporter strain of mice (*Axin2$^{CreERT2/+}$;R26R$^{mTmG/+}$*). A subset

of cells attached to the bone matrix were identified by their GFP-positive, Wnt-responsive status (Fig. 2M). Because GFP permanently labeled descendants of the original population, their fates could be followed over time. For example, after 7 days in the SRC (Fig. 2N) the new bone matrix that had formed was derived from Runx2-expressing descendants of the initial Wnt-responsive population (Fig. 2O). The Runx2-expressing cells were also immunopositive for Ki67 (Fig. 2P). Therefore, new bone arising from an autograft originated from proliferating, Wnt-responsive osteoprogenitor cells that were attached to the original material generated by the osseo-shaping instrument.

Wnt-responsive bone debris contributes to immediate post-extraction implant osseointegration

Bone debris is typically used when gaps exist around an implant e.g., in cases where an implant is placed immediately after tooth extraction. Viable cells attached to this material can be identified by their Wnt-responsiveness, but in a fresh extraction socket, there was another source of Wnt-responsive cells that had to be considered. The periodontal ligament (PDL; Fig. 3A) also harbors a population of GFP^{+ve} stem cells (Fig. 3B and see [23]). When the molar was extracted to allow implant placement, remnants of the PDL remained attached to the socket wall (Fig. 3C) and Wnt-responsive cells were detectable in these PDL remnants (Fig. 3D).

To examine the extent to which Wnt-responsive cells contributed to osseointegration, an immediate post-extraction implant was placed into a fresh extraction socket (Fig. 3E). Peri-implant gaps were filled with osseous coagulum, bone chips, and PDL remnants (Fig. 3F); the latter being identified by Periostin expression (Fig. 3F'). Bone chips generated by the osseo-shaping instrument were surrounded by Wnt-responsive osteoprogenitor cells (Fig. 3G), which eventually differentiated into ALP-producing osteoblasts (Fig. 3H).

Three-dimensional μCT imaging was used to determine the volume of the fresh extraction socket (Fig. 3I,I') as well as the volume occupied by the immediate post-extraction implant (Fig. 3I'). Then using FEA, the size of the peri-implant gap was calculated as ~2.85mm^3 (Fig. 3J). Thus, the space available around the implant was slightly larger than the volume of the implant itself, 2.2mm^3. This volume could be readily visualized by μCT (Fig. 3K) and volume rendering (Fig. 3L). After osseointegration occurred in the mouse model, the gap was occupied by bone comprised of GFP^{+ve} osteocytes (Fig. 3M).

A WNT therapeutic potentiates the osteogenic properties of bone chips in the peri-implant environment

A logical progression of the above data was to test whether locally increasing Wnt signaling around an immediate post-extraction implant would lead to faster osseointegration. A liposomal formulation of human recombinant WNT3A protein (L-WNT3A), or an identical liposomal formulation containing PBS, were delivered via peri-implant injection at the same time as implant placement; three days later, the distribution of proliferating cells, identified by PCNA IHC, were significantly greater in the L-WNT3A treated cases (compare 4A,B, quantified in C). Likewise, the distribution of osteoprogenitor cells, identified by Runx2

expression, also was significantly greater in the L-WNT3A versus the L-PBS treated cases (Fig. 4D,E, quantified in F).

On PID14, cases were analyzed for evidence of peri-implant bone formation. Imaging analyses revealed gaps between the implant and socket walls in the L-PBS treated cases (Fig. 4G). Gaps still existed around L-WNT3A treated implants (Fig. 4I) but compared to L-PBS, the L-WNT3A treated cases had higher levels of ALP expression (Fig. 4H,J, quantified in K). Histology coupled with histomorphometric analyses revealed that gaps still existed in both L-PBS and L-WNT3A cases (Fig. 4L,M), but the amount of peri-implant bone was significantly greater in L-WNT3A treated cases (Fig. 4N). Thus, dual treatment of bone chips and L-WNT3A in the peri-implant environment stimulated the proliferation of osteoprogenitor cells, which eventually resulted in faster gap closure around immediate post-extraction implants.

Discussion

Ensuring rapid new bone formation around an immediate post-extraction implant

Placing an implant into a fresh extraction socket implies that there will be peri-implant gaps. These gaps are initially filled with a blood clot; thereafter, Wnt-responsive stem cells originating from the PDL occupy the gaps and eventually give rise to new bone that contributes to implant osseointegration (Fig. 3 and [23]). In an attempt to accelerate healing, bone graft materials are often used to fill the gaps. The bone graft can be synthetic, xenogeneic autologous, or allogeneic. Regardless of the source, bone grafting adds time, cost, and increased risk of morbidity to the surgical procedure, oftentimes with questionable benefit[38, 39]. Here, we present a streamlined protocol that combines the steps of site preparation and gap-filling to accelerate new bone formation around an immediate post-extraction implant.

The osteogenic potential of bone chips relies on how they are generated and handled

Typical dental drills are designed to excavate bone debris from the osteotomy [40] because retention of the material can interfere with the flow of a coolant, resulting in thermal stress and drill damage to the surrounding bone [41]. If bone debris is generated by high speed drilling, then the heat generated causes osteocyte apoptosis and bone necrosis[21, 42], which reduces the osteogenic capacity of the material[43, 44]. If bone chips are collected by scraping bone surfaces (e.g. the ramus), then the material primarily consists of crushed cortical bone matrix with few viable cells[37, 45]. Even though some trabecular bone might also be harvested, especially at the edentulous maxilla – whose cortical plate is thinner[46] – new bone formation will most likely result from the release of growth factors from the matrix rather than cell activity[47]. The osseo-shaping instrument generates minimal heat, which obviates the need for irrigation[21]. Here we demonstrated that bone chips generated by the osseo-shaping instrument originate from both cortical and cancellous bone, and some of them are retained *in situ* i.e., in the fresh extraction socket and in gaps around the implant (Fig. 2). Molecular analyses demonstrated that much of this autologous material contained viable osteocytes enswathed with osteoprogenitor cells (Fig. 2). The autologous material

was generated as part of the osteotomy procedure; consequently, the need for a second surgical site was eliminated.

Exploiting the full potential of the peri-implant gap: L-WNT3A enhances the osteogenic properties of autologous bone chips

While the osteogenicity of fresh Human explants was demonstrated without any further treatment other than storage in saline[48, 49], here, we attempted to accelerate new bone formation in our rodent model. We first identified Wnt-responsive osteoprogenitor cells attached to autologous bone chips (Fig. 3). Wnt-responsive progenitor cells were also present in PDL remnants of the fresh extraction socket (Fig. 3 and [23]). Together, both progenitor populations contributed to new bone formation around immediate post-extraction implants (Fig. 3 and [50]). To increase these progenitor cell populations and accelerate bone formation, we treated the peri-implant environment with L-WNT3A. No additional biomaterial or exogenous matrices were required and compared to PBS controls, the WNT-treated peri-implant environment showed an early, significant increase in the number of proliferating osteoprogenitor cells (Fig. 4). This led to an increase in ALP expression and consequently, a significantly higher amount of bone in the peri-implant environment (Fig. 4). These data suggest the potential application of a WNT protein therapeutic for accelerating peri-implant bone formation.

Limitations of the study and conclusions

In this study, we were able to address the fate of bone chips generated by the osseo-shaping instrument, and directly compared them to conventional drill-generated chips and bone chips generated by handheld bone scrapers. Bone chips generated by bone scrapers were easier to collect and an *in vivo*, SRC analysis allowed us to conclude that compared to bone chips generated by the osseo-shaping instrument, bone chips generated by scraping were less osteogenic (Fig. 2). This is in keeping with other published reports, showing the bone chips generated by a scraper are preferable to those generated by a drill[8, 37]. Liposomal WNT3A delivered at the time of surgery further increased the osteogenic properties of autologous bone chips generated by the osseo-shaping instrument, and thus accelerated immediate post-extraction implant osseointegration.

There is a critically important limitation of this study. Animal models are intended to mimic, to the greatest degree possible, a patient response to treatment. We aligned our model with the target patient population i.e., those receiving immediate post-extraction implants, but notable knowledge gaps still remain to be answered: for example, if a Wnt therapeutic and an osseo-shaping instrument promote peri-implant bone formation as robustly in patients as they have in our animal model, then how does this translate into the clinical timeline to occlusal loading?

Supplementary Material

Refer to Web version on PubMed Central for supplementary material.

Acknowledgements & Conflict of interest

References

1. Robinson E Osseous coagulum for bone induction. J Periodontol 1969;40:503–510. [PubMed: 4899855]

2. Robinson RE. The osseous coagulum for bone induction technique. A review. J Calif Dent Assoc 1970;46:18–27. [PubMed: 4911837]

3. Albrektsson T Repair of bone grafts. A vital microscopic and histological investigation in the rabbit. Scand J Plast Reconstr Surg 1980;14:1–12. [PubMed: 6992262]

4. Gray JC, Elves MW. Donor cells' contribution to osteogenesis in experimental cancellous bone grafts. Clin Orthop Relat Res 1982:261–271.

5. Li J, Yin X, Huang L, et al. Relationships among Bone Quality, Implant Osseointegration, and Wnt Signaling. J Dent Res 2017;96:822–831. [PubMed: 28571512]

6. Baron R, Tross R, Vignery A. Evidence of sequential remodeling in rat trabecular bone: morphology, dynamic histomorphometry, and changes during skeletal maturation. Anat Rec 1984;208:137–145. [PubMed: 6711834]

7. Shapoff CA, Bowers GM, Levy B, Mellonig JT, Yukna RA. The effect of particle size on the osteogenic activity of composite grafts of allogeneic freeze-dried bone and autogenous marrow. J Periodontol 1980;51:625–630. [PubMed: 7007609]

8. Miron RJ, Hedbom E, Saulacic N, et al. Osteogenic potential of autogenous bone grafts harvested with four different surgical techniques. J Dent Res 2011;90:1428–1433. [PubMed: 21940523]

9. Pallesen L, Schou S, Aaboe M, Hjorting-Hansen E, Nattestad A, Melsen F. Influence of particle size of autogenous bone grafts on the early stages of bone regeneration: a histologic and stereologic study in rabbit calvarium. Int J Oral Maxillofac Implants 2002;17:498–506. [PubMed: 12182292]

10. Zaner DJ, Yukna RA. Particle size of periodontal bone grafting materials. J Periodontol 1984;55:406–409. [PubMed: 6086869]

11. Vignoletti F, Sanz-Esporrin J, Sanz-Martin I, Nunez J, Luengo F, Sanz M. Ridge alterations after implant placement in fresh extraction sockets or in healed crests: An experimental in vivo investigation. Clin Oral Implants Res 2019;30:353–363. [PubMed: 30864234]

12. Lee CT, Chiu TS, Chuang SK, Tarnow D, Stoupel J. Alterations of the bone dimension following immediate implant placement into extraction socket: systematic review and meta-analysis. J Clin Periodontol 2014;41:914–926. [PubMed: 24894299]

13. Vina-Almunia J, Candel-Marti ME, Cervera-Ballester J, et al. Buccal bone crest dynamics after immediate implant placement and ridge preservation techniques: review of morphometric studies in animals. Implant Dent 2013;22:155–160. [PubMed: 23462592]

14. Tonetti MS, Jung RE, Avila-Ortiz G, et al. Management of the extraction socket and timing of implant placement: Consensus report and clinical recommendations of group 3 of the XV European Workshop in Periodontology. J Clin Periodontol 2019;46 Suppl 21:183–194. [PubMed: 31215112]

15. Clementini M, Tiravia L, De Risi V, Vittorini Orgeas G, Mannocci A, de Sanctis M. Dimensional changes after immediate implant placement with or without simultaneous regenerative procedures: a systematic review and meta-analysis. J Clin Periodontol 2015;42:666–677. [PubMed: 26073267]

16. Caneva M, Botticelli D, Morelli F, Cesaretti G, Beolchini M, Lang NP. Alveolar process preservation at implants installed immediately into extraction sockets using deproteinized bovine bone mineral - an experimental study in dogs. Clin Oral Implants Res 2012;23:789–796. [PubMed: 22092470]

17. Sanz M, Lindhe J, Alcaraz J, Sanz-Sanchez I, Cecchinato D. The effect of placing a bone replacement graft in the gap at immediately placed implants: a randomized clinical trial. Clin Oral Implants Res 2017;28:902–910. [PubMed: 27273298]

18. Barrack RL. Bone graft extenders, substitutes, and osteogenic proteins. J Arthroplasty 2005;20:94–97.

19. Avila-Ortiz G, Chambrone L, Vignoletti F. Effect of Alveolar Ridge Preservation Interventions Following Tooth Extraction: A Systematic Review and Meta-Analysis. J Clin Periodontol 2019.

20. Baldwin P, Li DJ, Auston DA, Mir HS, Yoon RS, Koval KJ. Autograft, Allograft, and Bone Graft Substitutes: Clinical Evidence and Indications for Use in the Setting of Orthopaedic Trauma Surgery. J Orthop Trauma 2019;33:203–213. [PubMed: 30633080]

21. Chen CH, Coyac BR, Arioka M, et al. A Novel Osteotomy Preparation Technique to Preserve Implant Site Viability and Enhance Osteogenesis. J Clin Med 2019;8.

22. Karp NA, Meehan TF, Morgan H, et al. Applying the ARRIVE Guidelines to an In Vivo Database. PLoS Biol 2015;13:e1002151. [PubMed: 25992600]

23. Yuan X, Pei X, Zhao Y, Tulu US, Liu B, Helms JA. A Wnt-Responsive PDL Population Effectuates Extraction Socket Healing. J Dent Res 2018:22034518755719.

24. Porter AG, Janicke RU. Emerging roles of caspase-3 in apoptosis. Cell Death Differ 1999;6:99–104. [PubMed: 10200555]

25. Elmore S Apoptosis: a review of programmed cell death. Toxicol Pathol 2007;35:495–516. [PubMed: 17562483]

26. Jing W, Smith AA, Liu B, et al. Reengineering autologous bone grafts with the stem cell activator WNT3A. Biomaterials 2015;47:29–40. [PubMed: 25682158]

27. Soleimani M, Nadri S. A protocol for isolation and culture of mesenchymal stem cells from mouse bone marrow. Nat Protoc 2009;4:102–106. [PubMed: 19131962]

28. Sen N, Das BB, Ganguly A, et al. Camptothecin induced mitochondrial dysfunction leading to programmed cell death in unicellular hemoflagellate Leishmania donovani. Cell Death Differ 2004;11:924–936. [PubMed: 15118764]

29. Kalu DN. The ovariectomized rat model of postmenopausal bone loss. Bone Miner 1991;15:175–191. [PubMed: 1773131]

30. Leucht P, Jiang J, Cheng D, et al. Wnt3a reestablishes osteogenic capacity to bone grafts from aged animals. J Bone Joint Surg Am 2013;95:1278–1288. [PubMed: 23864176]

31. Kerbel RS. A Decade of Experience in Developing Preclinical Models of Advanced- or Early-Stage Spontaneous Metastasis to Study Antiangiogenic Drugs, Metronomic Chemotherapy, and the Tumor Microenvironment. Cancer J 2015;21:274–283. [PubMed: 26222079]

32. Krajewski S, Wechsler W. Development of subrenal capsule tumours following transplantation of rat RN6 multicell spheroids. J Neurooncol 1991;10:219–231. [PubMed: 1716672]

33. Cunha GR, Baskin L. Use of sub-renal capsule transplantation in developmental biology. Differentiation 2016;91:4–9. [PubMed: 26639079]

34. Colnot C, Lu C, Hu D, Helms JA. Distinguishing the contributions of the perichondrium, cartilage, and vascular endothelium to skeletal development. Dev Biol 2004;269:55–69. [PubMed: 15081357]

35. Szot GL, Koudria P, Bluestone JA. Transplantation of pancreatic islets into the kidney capsule of diabetic mice. Journal of visualized experiments : JoVE 2007:404. [PubMed: 18989445]

36. Dhamdhere GR, Fang MY, Jiang J, et al. Drugging a stem cell compartment using Wnt3a protein as a therapeutic. PLoS One 2014;9:e83650. [PubMed: 24400074]

37. Miron RJ, Gruber R, Hedbom E, et al. Impact of bone harvesting techniques on cell viability and the release of growth factors of autografts. Clin Implant Dent Relat Res 2013;15:481–489. [PubMed: 22375920]

38. Spinato S, Agnini A, Chiesi M, Agnini AM, Wang HL. Comparison between graft and no-graft in an immediate placed and immediate nonfunctional loaded implant. Implant Dent 2012;21:97–103. [PubMed: 22382749]

39. Verdugo F, Laksmana T, D'Addona A, Uribarri A. Facial cortical bone regeneration post-extraction in non-grafted sockets allows for early implant placement and long-term functional stability. Arch Oral Biol 2020;112:104678. [PubMed: 32062103]

40. Childs T Metal machining : theory and applications. London : Wiley; 2000: viii, 408 p.

41. Boothroyd G Fundamentals of metal machining and machine tools. Washington: Scripta Book Co.; 1975: xxix, 350 p.

42. Wang L, Aghvami M, Brunski J, Helms J. Biophysical regulation of osteotomy healing: An animal study. Clin Implant Dent Relat Res 2017;19:590–599. [PubMed: 28608504]

43. Atari M, Chatakun P, Ortiz O, et al. Viability of maxillary bone harvesting by using different osteotomy techniques. A pilot study. Histol Histopathol 2011;26:1575–1583. [PubMed: 21972096]

44. Miron RJ, Bosshardt DD, Laugisch O, et al. In vitro evaluation of demineralized freeze-dried bone allograft in combination with enamel matrix derivative. J Periodontol 2013;84:1646–1654. [PubMed: 23347347]

45. Maridati P, Dellavia C, Pellegrini G, Canciani E, Maragno A, Maiorana C. Histologic and Radiographic Comparison of Bone Scraper and Trephine Bur for Autologous Bone Harvesting in Maxillary Sinus Augmentation. Int J Oral Maxillofac Implants 2015;30:1128–1136. [PubMed: 26394350]

46. Katranji A, Misch K, Wang HL. Cortical bone thickness in dentate and edentulous human cadavers. J Periodontol 2007;78:874–878. [PubMed: 17470021]

47. Zimmermann M, Caballe-Serrano J, Bosshardt DD, Ankersmit HJ, Buser D, Gruber R. Bone-Conditioned Medium Changes Gene Expression in Bone-Derived Fibroblasts. Int J Oral Maxillofac Implants 2015;30:953–958. [PubMed: 26252049]

48. Verdugo F, Saez-Roson A, Uribarri A, et al. Bone microbial decontamination agents in osseous grafting: an in vitro study with fresh human explants. J Periodontol 2011;82:863–871. [PubMed: 21138353]

49. Mailhot JM, Borke JL. An isolation and in vitro culturing method for human intraoral bone cells derived from dental implant preparation sites. Clinical oral implants research 1998;9:43–50. [PubMed: 9590944]

50. Pei X, Wang L, Chen C, Yuan X, Wan Q, Helms JA. Contribution of the PDL to Osteotomy Repair and Implant Osseointegration. J Dent Res 2017;96:909–916. [PubMed: 28481696]
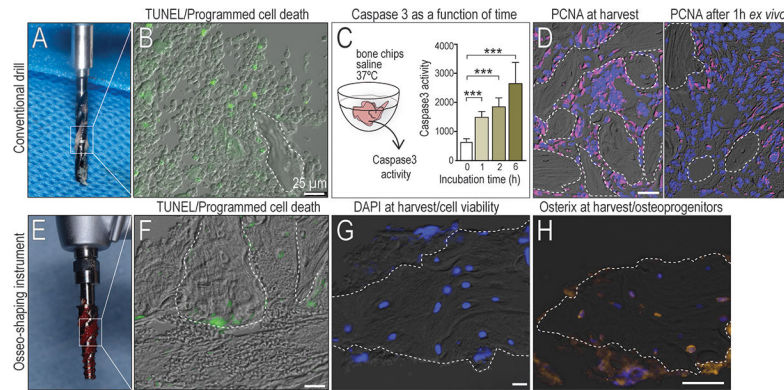
Figure 1. Bone chip viability is impacted by time outside the body.
(A) Autologous bone chips are typically harvested as surgical debris from the cutting flutes of a drill, then held outside the body. (B) Immediately after harvest, TUNEL staining detects cells undergoing apoptosis. (C) Caspase3 activity as a readout of cellular apoptosis in bone grafts, measured as a function of time. (D) PCNA immunostaining in the autograft (left) immediately after harvest, and (right) 1h after harvest. (E) A miniaturized osseo-shaping instrument, after removal from an osteotomy (F) TUNEL staining to detect programmed cell death, (G) DAPI staining to detect viable cells; and (H) Osterix IHC to identify osteoprogenitors in and around representative in situ bone chips. Scale bars = 25 μm. Data are means ± SD, ***p < 0.01. In all panels, a dotted line demarcates the bone chip.
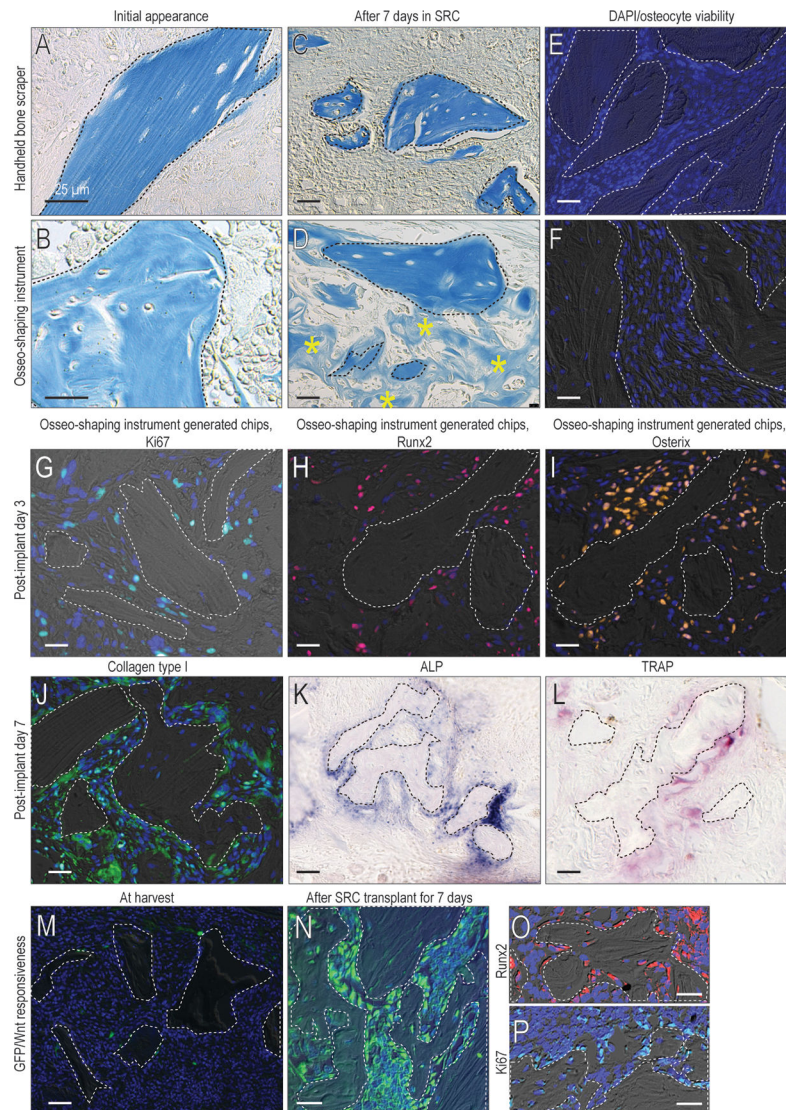
Figure 2. The osseo-shaping instrument generates viable bone chips that retain their biological activity in situ.
(A) Aniline blue staining of bone scraper generated chips and the (B) osseo-shaping instrument generated bone chips at time of harvest, and (C, D) 7 days after transplantation in the sub-renal capsule. (E) DAPI staining for osteocyte viability in bone scraper generated chips and the (F) osseo-shaping instrument generated bone chips. (G) On post-surgery day 3, representative IHC for the cell proliferation marker Ki67, and for the osteogenic markers (H) Runx2 and (I) Osterix. (J) On post-surgery day 7, representative IHC for Collagen type I, and (K) for ALP and (L) TRAP activities. (M) Freshly generated bone chips from Axin2$^{CreERT2/+}$;R26R$^{mTmG/+}$ mice and stained for GFP to identify Wnt-responsive cells and (N) the same bone chips after 7 days in the sub-renal capsule stained for GFP and (O) Runx2 and (P) Ki67. Dotted lines demarcate freshly generated bone chips and yellow asterisks indicate new bone. (N) Bone chips harvested (O) The osteoprogenitor protein Runx2 and (P) the cell proliferation marker Ki67 co-localize with the GFP^{+ve}, Wnt-responsive cells. Scale bars = 25μm. In all panels, a dotted line demarcates the bone chip.
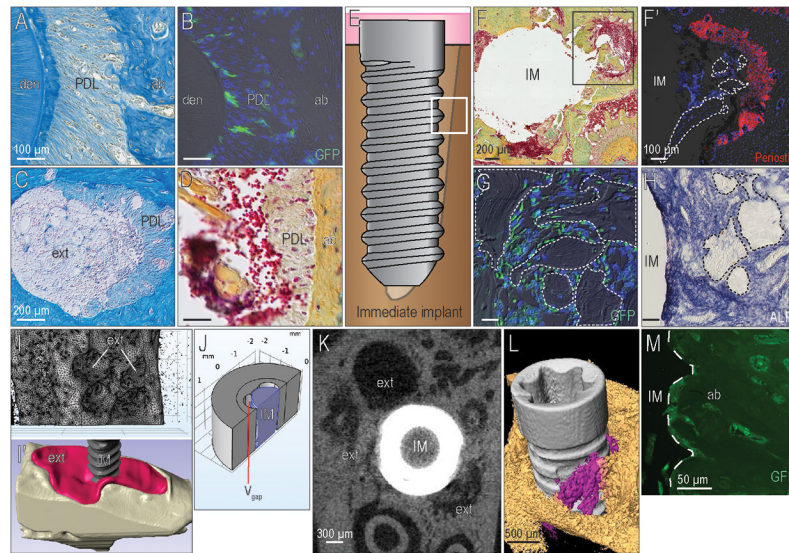
Figure 3. Exploiting the osteogenic potential of bone chips in an immediate post-extraction implant surgery.

(A) At the periodontal interface (B) a subset of cells in the PDL are GFP-expressing, Wnt-responsive stem cells. (C) Once a tooth is extracted, PDL remnants remain attached to the bundle bone. (D) The presence of PDL remnants was confirmed by Pentachrome staining. (E) When an immediate post-extraction implant bed was prepared, the gap regions (boxed area) (F) were filled with bone chips; PDL remnants also existed. (F') PDL remnants were identified by their Periostin immunopositivity. (G) Within 3 days, bone chips generated by the osseo-shaping instrument were surrounded by GFP^{+ve}, Wnt-responsive osteoprogenitor cells that (H) by day 7 had given rise to ALP^{+ve}, mineralizing matrix in the peri-implant environment. (I) Calculation of the gap volume between the implant and the socket walls, which (I') corresponded to the extraction socket volume also shown in a 3D reconstruction of the extraction socket (red) with the immediate post-extraction implant. (J) The volume of the gap, V_{gap}, was calculated in COMSOL (see Methods and Supplementary Figure in online Journal of Periodontology). (K) 2D and (L) 3D μCT images, demonstrating the gaps between the extraction socket walls and the implant; some of the V_{gap} was occupied by autologous bone chips (purple). (M) Using Axin2$^{CreERT2/+}$;R26R$^{mTmG/+}$ mice, the origin of the peri-implant bone was confirmed to have arisen from GFP^{+ve}, Wnt-responsive cells. Abbreviations: den, dentin; PDL, periodontal ligament; ab, alveolar bone; ext, extraction socket; IM, implant; ALP, alkaline phosphatase. Scale bars = 100μm (A,B,F'-H), 200μm (C,D,F), 300μm (K), 500μm (L), 50μm (M). In panels F', G, H, a dotted line demarcates the bone chip. In panel M a dotted line demarcates the implant.
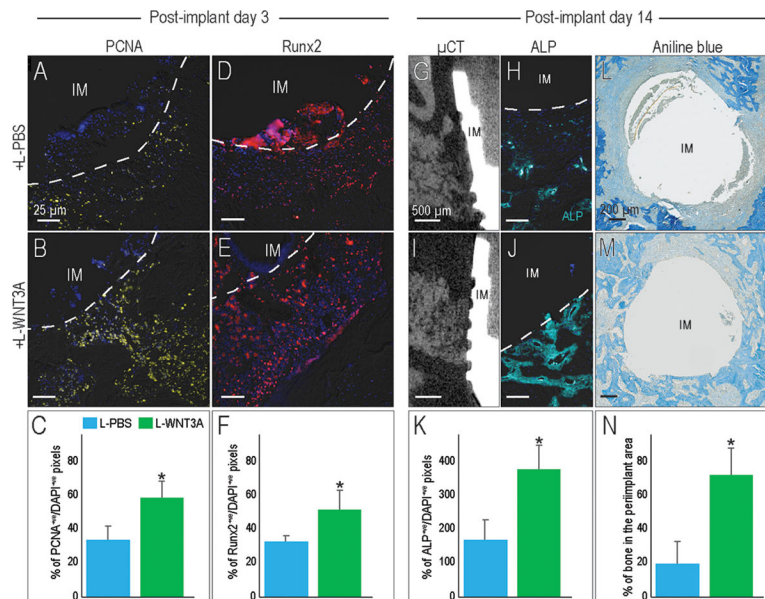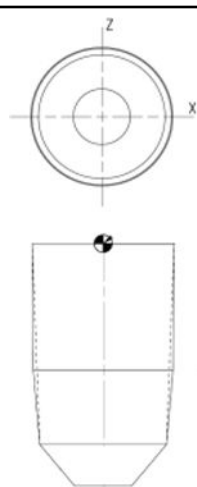
Figure 4. L-WNT3A amplifies the osteogenic potential of peri-implant bone chips that contribute to osseointegration.

PCNA expression in the peri-implant environment on PID3, in response to (A) L-PBS or (B) L-WNT3A, quantified in (C). Runx2 expression in the peri-implant environment on PID3, in response to (C) L-PBS or (D) L-WNT3A, quantified in (F). L-PBS treated sites on PID14, analyzed using (G) sagittal µCT of the bone-implant interface. (H) A representative transverse tissue section showing ALP IHC. L-WNT3A treated sites on PID14, analyzed by (I) µCT and (J) ALP IHC, quantified in (K). On PID14, aniline blue histology of the (L) L-PBS treated and (M) L-WNT3A-treated sites. (N) Quantification of new peri-implant bone on PID14. Abbreviations: PID, post-implant day; IM, implant, Scale bars = 25µm (A-E, H, J); 500µm (G,I); 200µm (L-M). Data are means ± SD, n = 4 per group, *p < 0.05. In panels A, B, D, E, H, J, a dotted line demarcates the implant.

Table 1:

Instruments and their characteristics used in this study.

	Rat rattus		*Mus musculus*	
	Step	**Diameter (mm)**	**Step**	**Diameter (mm)**
Conventional osteotomy	1	0.8	1	0.33
	2	1.0	2	0.55
	3	1.2	-	-
Osseo-shaping instrument osteotomy	1	0.8	1	0.33
	2	1.33	2	0.55
Implant for…	Shape	Crestal diameter	Apical diameter	Drawing
Rat rattus	Round	1.38	1.25	
Rat rattus	Tri-oval$_{mini}$	1.46	1.25	
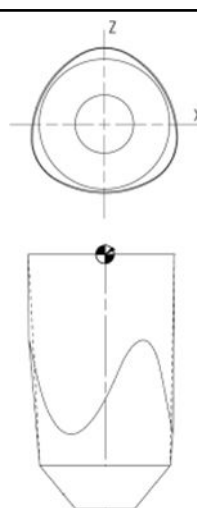
Table 2:

Distribution of animals and analyses carried out in this study.

Sample size (N)	Source of bone graft	Time of incubation after harvest (hours)	Type of analysis	Timepoint of analysis	Shown in
3	Mouse mxM1 healed site	0	TUNEL	immediately after harvest	Fig. 1B
3	Mouse mxM1 healed site	0, 1	PCNA IHC, DAPI	post-transplant day 3	Fig. 1D
5	Osseo-shaping instrument-produced osseous coagulum	0	TUNEL, DAPI, IHC, histology	post-implant day 0	Fig. 1F–H Fig. 2B
5	Handheld bone scraper-produced bone chips	0	Histology, DAPI	post-implant day 0 post-implant day 7	Fig. 2A Fig. 2C,E
5	Osseo-shaping instrument-produced osseous coagulum	0	IHC	post-implant day 3	Fig. 2G–I
5	Osseo-shaping instrument-produced osseous coagulum	0	histology, DAPI, IHC, TRAP, ALP	post-implant day 7	Fig. 2D,F,J–L
3	osseous coagulum	0	IHC	post-transplant day 0 post-transplant day 7	Fig. 2M Fig. 2N–P
Sample size (N)	Site	rodent species	Type of analysis	Timepoint of analysis	Shown in
>20	intact PDL	rat, mouse	histology	Intact state	Fig. 3A, B
>20	fresh extraction socket	rat, mouse	histology	Intact state	Fig. 3C,D
>10	extraction socket gap area around an immediate implant	rat	histology, IHC, ALP	post-implant day 0	Fig. 3F,F'
>10	extraction socket gap area around an immediate implant	mouse	IHC	post-implant day 7	Fig. 3G,M
>10	extraction socket gap area around an immediate implant	rat	ALP, µCT	post-implant day 0	Fig. 3H,K,L
3	extraction socket gap area around an immediate implant +L-PBS	rat	IHC, µCT, histology	post-implant day 3, post-implant day 14	Fig. 4A,C,E,F,I
4	extraction socket gap area around an immediate implant +L-WNT3A	rat	IHC, µCT, histology	post-implant day 3, post-implant day 14	Fig. 4B,D,G,H,J